PHYSICAL REVIEW B **68**, 220101(R) (2003)

Image reconstruction of nanostructured nonperiodic objects only from oversampled hard x-ray diffraction intensities

Yoshinori Nishino,[1] Jianwei Miao,[2] and Tetsuya Ishikawa[1]
[1]*SPring-8/RIKEN, 1-1-1 Kouto, Mikazuki, Sayo, Hyogo 679-5148, Japan*
[2]*Stanford Synchrotron Radiation Laboratory, Stanford Linear Accelerator Center, Stanford University, Stanford, California 94309-0210, USA*

(Received 22 September 2003; published 24 December 2003)

X-ray-diffraction microscopy images nanocrystals and nonperiodic objects by directly reconstructing from oversampled diffraction intensities. Successful image reconstruction of nonperiodic objects has so far required additional experiments to supplement the missing data in the diffraction intensities. Reconstruction only from diffraction data is desirable. We show that image reconstruction of nonperiodic objects can be done without any supplemental experiments by applying a modified hybrid input-output algorithm to experimental hard x-ray-diffraction data of a nanostructured pattern.

DOI: 10.1103/PhysRevB.68.220101 PACS number(s): 61.10.−i, 07.85.Tt, 41.50.+h

X-ray-diffraction microscopy is a newly developed imaging technique to determine the structures of nonperiodic objects and nanocrystals by using coherent x rays and the oversampling method.[1–9] When a coherent beam of x rays illuminates a finite object, the Fraunhofer diffraction intensities of the object can be sampled at a spacing finer than the Nyquist interval. When the sampling interval is fine enough so that the oversampling ratio, a parameter to characterize the degree of oversampling, is 2 or more, a nontrivial unique phase set is in principle embedded inside the diffraction intensities,[10] and can be directly retrieved by using global minimization methods such as an iterative method.[11] Fienup's hybrid input-output (HIO) algorithm shows good convergence among algorithms of the iterative methods.[12] Due to a high penetrating power of x rays, x-ray-diffraction microscopy can be applied to imaging relatively thick objects. Furthermore the method does not require x-ray optics with a high numerical aperture and can achieve higher spatial resolution than conventional x-ray imaging methods. These features make it potentially an important imaging technique with broad application in nanomaterials science[3,4,6–9] and biology.[5,13]

In x-ray-diffraction microscopy, missing near-forward diffraction data due to a beamstop have been a major difficulty that has been preventing us from reconstructing nonperiodic objects only from the diffraction intensities. The missing data problem is essentially unavoidable, since the unscattered transmitted x rays contribute in addition to the diffracted x rays, and hence the diffraction intensities at the exact forward pixels are not directly observable. The beamstop has to be sufficiently large not to overload the detector with a limited dynamic range. Furthermore, the parasitic scattering, e.g., from a pinhole, also makes it difficult to measure near-forward data with a high signal-to-noise ratio.

The near-forward data correspond to low spatial frequencies of the electron density of the sample, and determine an approximate shape of the reconstructed image. In previous works Fourier transform of lower resolution images by, e.g., soft x-ray microscopes[14] was used to estimate the near-forward diffraction intensities.[3–5] It should however be noted that the estimated intensities were somewhat different from the correct ones, because soft x-ray microscopes only provide absorption contrast images. In another work, a scanning electron microscope image was used to define a detailed shape of the support.[9] Here a support is the region where the sample electrons are expected to exist, and is needed to be defined for image reconstruction. When a sample consists of a small number of isolated pieces, the autocorrelation (Patterson) function can be used to define the support,[9] but the technique is difficult to be applied to general objects with complex structures. Also near-forward data are necessary to calculate the autocorrelation function, and hence the missing data problem can not be avoided. If a sample has spatial periodicity such as a nanocrystal, the problem can be circumvented by recording diffraction intensities near a Bragg peak.[6,7] In this experimental setup, measurement is relatively easier due to less contribution of the parasitic scattering and no contribution of the transmitted x rays.

The loss of near-forward data is an extremely challenging problem in practical applications of x-ray-diffraction microscopy. The required supplemental experiments to recover near-forward data take extra time for measurement and hence cause extra sample damage. The sample damage problem is especially crucial in biological applications.[15] With x-ray free electron lasers, serious sample damage may not allow us to perform supplemental experiments.[16] In time-resolved experiments to follow structure changes, it will be difficult to carry out supplemental experiments with the same sample condition. In this paper we show that image reconstruction of nonperiodic objects can be carried out without requiring any supplemental experiments by applying the modified HIO (MHIO) algorithm to simulated data and experimental hard x-ray-diffraction data of a nanostructured pattern.

In the iterative methods, the phases are recovered by iteratively applying Fourier transform and inverse Fourier transform. At each iteration, constraints are applied in both reciprocal space and real space. In reciprocal space, the absolute values of the estimated structure factor $G_n(\boldsymbol{K})$ are set to the experimental values $|F(\boldsymbol{K})|$ while keeping the estimated phases. The constrained structure factor $G_n'(\boldsymbol{K})$ is thus given by

$$G_n'(\boldsymbol{K}) = \begin{cases} G_n(\boldsymbol{K}), & \boldsymbol{K} \notin D \\ m_n(\boldsymbol{K}) G_n(\boldsymbol{K}), & \boldsymbol{K} \in D, \end{cases} \tag{1}$$

where

$$m_n(\boldsymbol{K}) = \frac{|F(\boldsymbol{K})|}{|G_n(\boldsymbol{K})|}, \tag{2}$$

n is the iteration number and $\boldsymbol{K}$ the scattering vector. D denotes the region in reciprocal space where experimental data exist. The inverse Fourier transform of $G_n'(\boldsymbol{K})$ provides the electron density $\rho_n'(\boldsymbol{r})$. A real-space constraint is applied to $\rho_n'(\boldsymbol{r})$ by setting the electron density gradually to zero for those pixels outside the support or where the estimated electron density is negative. There are different algorithms for the real-space constraints. In Fienup's HIO algorithm,[12] the constrained electron density $\rho_{n+1}(\boldsymbol{r})$ is obtained by

$$\rho_{n+1}(\boldsymbol{r}) = \begin{cases} \rho_n'(\boldsymbol{r}) & (\boldsymbol{r} \in S) \wedge [\rho_n'(\boldsymbol{r}) \geqslant 0] \\ \rho_n(\boldsymbol{r}) - \beta \rho_n'(\boldsymbol{r}), & \text{otherwise,} \end{cases} \tag{3}$$

where S represents the support region and β is a constant typically between 0.5 and 1.

The iterative method starts with a guessed electron density $\rho_i(\boldsymbol{r})$ as the initial input. In the studies, we used for $\rho_i(\boldsymbol{r})$ a random electron density inside the support and no electron density outside the support. Here a problem arises in the normalization of $\rho_i(\boldsymbol{r})$. The total number of electrons in a sample is unknown when the diffraction intensity at the central pixel is unknown. This is because the structure factor at the central pixel determines the total number of electrons. We propose to normalize the Fourier transform $G_i(\boldsymbol{K})$ of $\rho_i(\boldsymbol{r})$. The normalization is made so as to equalize the maximum of $G_i(\boldsymbol{K})$ in $\boldsymbol{K} \in D$ to the experimental value,

$$G_0(\boldsymbol{K}) = \begin{cases} tG_i(\boldsymbol{K}), & \boldsymbol{K} \notin D \\ m_i(\boldsymbol{K}) G_i(\boldsymbol{K}), & \boldsymbol{K} \in D, \end{cases} \tag{4}$$

where

$$t = \frac{\max(|F(\boldsymbol{K})|)_{\boldsymbol{K} \in D}}{\max(|G_i(\boldsymbol{K})|)_{\boldsymbol{K} \in D}}, \tag{5}$$

and $m_i(\boldsymbol{K})$ is given by Eq. (2) with $n = i$. The inverse Fourier transform of $G_0(\boldsymbol{K})$ finally gives the normalized initial electron density $\rho_0(\boldsymbol{r})$.

In order to clarify the problem of the HIO algorithm with missing near-forward data, we first carried out reconstructions with simulated data. We took an image shown in Fig. 1(a) as a two-dimensional real sample with 91×45 pixels. Figure 1(b) shows simulated diffraction intensities with 129×129 pixels. The diffraction data at the central 37×37 pixels were removed to simulate the data loss due to a beamstop. In Fig. 1(b) the diffraction intensities were oversampled, which corresponds to surrounding the electron density area with a no-density area. The support size was set to the same as the image size (a tight support). The oversampling ratio, defined by $\sigma = (\text{total area})/(\text{support area})$,[10] was 4.0. β in Eq. (3) was set to be, throughout the analyses, 0.6 in the top and left regions outside the support and 0.8 otherwise. We used Eq. (4) for the normalization of the initial electron density. The image reconstruction using the HIO algorithm was not successful as shown in Fig. 1(c). Figure 2 (a) shows the reconstruction error as a function of the iteration number, which is defined by

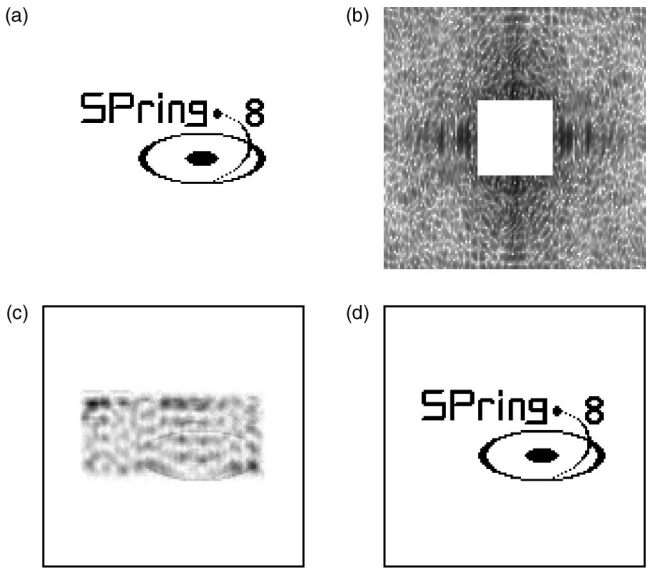

FIG. 1. Simulations of image reconstruction. (a) Original image in 91×45 pixels. (b) Simulated oversampled diffraction intensities in 129×129 pixels. The data at the central 37×37 pixels were removed. The reconstructed images after 2×10^4 iterations are shown in (c) for the HIO algorithm and in (d) for the MHIO algorithm. The data are shown in a linear gray scale for (a), (c), and (d); and in a logarithmic gray scale for (b). The black frames around the images of (c) and (d) indicate the total reconstruction areas.

$$E_n = \left(\sum_{\boldsymbol{r} \notin S} |\rho_n'(\boldsymbol{r})|^2 \Big/ \sum_{\boldsymbol{r} \in S} |\rho_n'(\boldsymbol{r})|^2 \right)^{1/2}. \tag{6}$$

Although the reconstruction error in the HIO algorithm gradually decreased with the iteration number, it does not guarantee that the reconstruction proceeded toward the correct solution. As shown in Fig. 2(b), the estimated total number of electrons increased with the iteration number, which reduced the reconstruction error. But the quality of the recon-

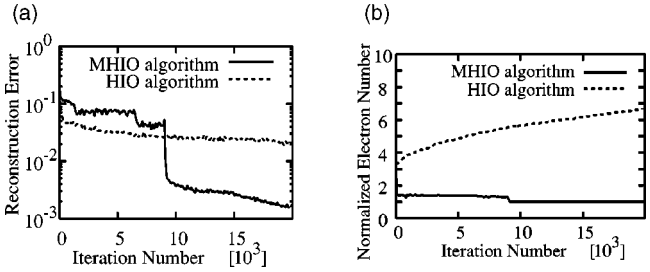

FIG. 2. Convergence of the image reconstruction for the simulations shown in Fig. 1. (a) The reconstruction errors and (b) the estimated total numbers of electrons normalized to the true values are shown as a function of the iteration number. The estimated total number of electrons approached to the true value only in the MHIO algorithm.

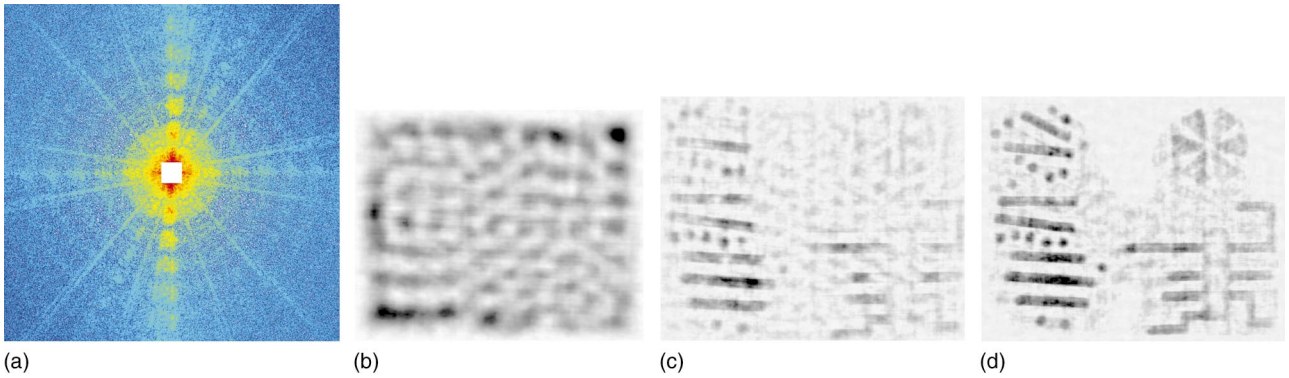

FIG. 3. (Color) Image reconstruction from the experimental diffraction data of a nanostructured pattern. (a) Oversampled diffraction intensities in 1001×1001 pixels. The data at the central 61×61 pixels were missing due to a beamstop. The reconstructed images in the central 363×290 pixels (2.6×2.0 μm^2) after 5×10^4 iterations are shown in (b) for the HIO algorithm, in (c) for the MHIO algorithm, and in (d) for the MHIO algorithm with an improved support defined using (c). The single pixel size of the reconstructed images is 7×7 nm^2.

structed image did not improve. The increase of the estimated total number of electrons with the iteration number in the HIO algorithm is generally observed when the missing near-forward data region is large, and which results in the failure of the HIO algorithm.

The failure of the HIO algorithm in the above example was caused by the fact that there are no constraints to make the estimated total number of electrons converge to the true value. We therefore iteratively normalized the total number of electrons by multiplying a factor to the estimated structure factor at the central pixel $G_n(\mathbf{0})$,

$$G_n'(\mathbf{0}) = m_n^{(0)} G_n(\mathbf{0}), \tag{7}$$

where

$$m_n^{(0)} = \alpha\left(\frac{1}{\overline{m}_n} - 1\right) + 1, \tag{8}$$

$\overline{m}$ is the average of $m_n(\boldsymbol{K})$ over $\boldsymbol{K}\in D$, and α is a constant typically between 0.5 and 1. When the estimated diffraction pattern is shaper than the experimental one, $\overline{m}_n$ is smaller than unity and consequently $m_n^{(0)}$ is larger than unity. Conversely when the estimated diffraction pattern is broader than the experimental one, $\overline{m}_n$ is larger than unity and consequently $m_n^{(0)}$ is smaller than unity. Therefore the iterative normalization factor of Eq. (7) has an effect to decrease the diffraction intensity at the central pixel when the estimated diffraction pattern is sharper than the experimental one, and increase it when the estimated diffraction pattern is broader. The criterion to determine whether the estimated diffraction pattern is sharper or broader than the experimental one does not include the missing near-forward data. We call the HIO algorithm with the initial normalization of Eq. (4) and the iterative normalization of Eq. (7) the MHIO algorithm.

We applied the MHIO algorithm to the simulated diffraction data in Fig. 1(b), and set $\alpha=0.5$ throughout the analyses. As shown in Fig. 1(d), the image was almost perfectly reconstructed after 2×10^4 iterations using the MHIO algorithm. The estimated total number of electrons in the MHIO algorithm approached the true value as shown in Fig. 2(b) due to the iterative normalization factor of Eq. (7). Note that in both simulations using the HIO and MHIO algorithms, we used the same initial electron density, and the initial total number of electrons was 3.3 times higher than the true value. The estimated total number of electrons changed rapidly to 1.5 times higher than the true value after the first 50 iterations of the MHIO algorithm. Reasonable reconstruction using the HIO algorithm was obtained after 2×10^4 iterations when the missing near-forward data size was up to 9×9 pixels, which was 17 times smaller than that of the MHIO algorithm.

We then applied the HIO and MHIO algorithms to experimental hard x-ray-diffraction data. The experiment was performed at BL29XUL (Ref. 17) of SPring-8 using the same experimental setup as the one used in Refs. 4, 5, and 18. A two-dimensional nanostructured gold pattern with the size of 2.5×2.0 μm^2 was used as a sample [see Fig. 2(a) of Ref. 18 for the scanning electron microscopy image]. The sample was made on a Si_3N_4 membrane by electron-beam lithography. Hard x-rays with a wavelength of 2.13 Å were used to achieve high spatial resolution. In x-ray-diffraction microscopy experiments, coherent x-rays are required. The condition for the transverse coherence is $(\Delta\theta)_{\mathrm{rms}} \leqslant \lambda/(4\pi O a)$, and for the longitudinal coherence is $(\Delta\lambda/\lambda)_{\mathrm{FWHM}} \leqslant \sqrt{2\ln 2}\, d/(\pi O a)$. Here $\Delta\theta$ is the angle that the source subtends at the sample, λ the wavelength, O the oversampling degree, a the sample size, and d the desired single pixel size of the reconstructed image. In our case the conditions were $(\Delta\theta)_{\mathrm{rms}} \leqslant 2.4$ μrad and $(\Delta\lambda/\lambda)_{\mathrm{FWHM}} \leqslant 3.7\times10^{-4}$. The required transverse coherence was achieved by a small vertical source size (~10 μm) (Ref. 19) and by setting the horizontal front-end slit size to be 150 μm (rms: 43 μm), where the x-ray source and the front-end slit were located at 54-m and 25-m upstream of the sample, respectively. The required longitudinal coherence was achieved by using a Si (111) double-crystal monochromator with $(\Delta\lambda/\lambda)_{\mathrm{FWHM}} = 1.3\times10^{-4}$. A 20 μm diameter pinhole and a corner were placed at 38.1-mm and 12.7-mm upstream of the sample, respectively, to reduce the background scattering from the Si_3N_4 mem-

brane and to reduce the parasitic scattering from the pinhole. The diffraction intensities were measured by a direct illumination liquid-nitrogen-cooled charge-coupled device (CCD) detector with 1152×1242 pixels placed at 743-mm downstream of the sample. The single pixel size of the CCD detector was 22.5×22.5 μm^2. Due to a beamstop in front of the CCD detector, data were missing at some pixels. Part of the missing data was recovered by using centrosymmetry of the diffraction pattern (Friedel's law), but the data at the central 61×61 pixels were still lost after the symmetry operation.

Figure 3(a) shows the experimental diffraction pattern (1001×1001 pixels) with missing data at the central 61×61 pixels. The data are those used in Ref. 18. The size of the diffraction pattern and other experimental parameters determined the single pixel size of the reconstructed image to be 7×7 nm^2. The support size was set to be 2.6×2.0 μm^2 (363×290 pixels). The oversampling ratio was calculated to be $\sigma=9.5$. Figure 3(b) shows the reconstructed image after 5×10^4 iterations using the HIO algorithm with the initial normalization of Eq. (4), which was not recognizable. This is because the estimated total number of electrons, as observed in the simulations, increased with the iteration number, which indicates that the reconstructed image using the HIO algorithm did not improve with the iteration number. Figure 3(c) shows the recognizable reconstructed image of the sample pattern by using the MHIO algorithm. The estimated total number of electrons converged to a certain value in the MHIO algorithm. To refine reconstruction we used a lower quality reconstructed image of Fig. 3(c) to set an improved support. Figure 3(d) shows a reconstructed image with an improved support in the MHIO algorithm after 5×10^4 iterations. The improved support was defined as the region where the value of the Gaussian filtered image of Fig. 3(c) with sigma$=$20 pixels was more than 23% of the maximum of the Gaussian filtered image. Farther refinement can be done in a similar manner.

In summary, we have successfully reconstructed the image of a two-dimensional nanostructured pattern only from the oversampled hard x-ray-diffraction intensities with missing near-forward data by using the MHIO algorithm. The algorithm does not require additional experiments to supplement the missing intensities for x-ray-diffraction microscopy, and consequently reduces radiation damage to samples. We anticipate that the algorithm will greatly broaden the applications of x-ray-diffraction microscopy, especially in biological applications, in time-resolved measurement, and in measurement with x-ray free electron lasers, where it is difficult to supply the missing near-forward data with supplemental experiments.

We thank Dr. Y. Kohmura, Dr. K. Tamasaku, and Dr. M. Yabashi for their help in data acquisition. This work was supported by RIKEN and by the U.S. Department of Energy, Office of Basic Energy Sciences.

[1] D. Sayre, Acta Crystallogr. **5**, 843 (1952).
[2] D. Sayre, in *Direct Methods of Solving Crystal Structures*, edited by H. Schenk (Plenum Press, New York, 1991), p. 353.
[3] J. Miao, P. Charalambous, J. Kirz, and D. Sayre, Nature (London) **400**, 342 (1999).
[4] J. Miao, T. Ishikawa, B. Johnson, E.H. Anderson, B. Lai, and K.O. Hodgson, Phys. Rev. Lett. **89**, 088303 (2002).
[5] J. Miao, K.O. Hodgson, T. Ishikawa, C.A. Larabell, M.A. LeGros, and Y. Nishino, Proc. Natl. Acad. Sci. U.S.A. **100**, 110 (2003).
[6] I.K. Robinson, I.A. Vartanyants, G.J. Williams, M.A. Pfeifer, and J.A. Pitney, Phys. Rev. Lett. **87**, 195505 (2001).
[7] G.J. Williams, M.A. Pfeifer, I.A. Vartanyants, and I.K. Robinson, Phys. Rev. Lett. **90**, 175501 (2003).
[8] U. Weierstall, Q. Chen, J.C.H. Spence, M.R. Howells, M. Isaacson, and R.R. Panepucci, Ultramicroscopy **90**, 171 (2002).
[9] H. He, S. Marchesini, M. Howells, U. Weierstall, G. Hembree, and J.C.H. Spence, Acta Crystallogr., Sect. A: Found. Crystallogr. **59**, 143 (2003).
[10] J. Miao, D. Sayre, and H.N. Chapman, J. Opt. Soc. Am. A **15**, 1662 (1998).
[11] R.W. Gerchberg and W.O. Saxton, Optik (Stuttgart) **35**, 237 (1972).
[12] J.R. Fienup, Appl. Opt. **21**, 2758 (1982).
[13] J. Miao, K.O. Hodgson, and D. Sayre, Proc. Natl. Acad. Sci. U.S.A. **98**, 6641 (2001).
[14] J. Kirz, C. Jacobsen, and M. Howells, Q. Rev. Biophys. **28**, 33 (1995).
[15] R. Henderson, Q. Rev. Biophys. **28**, 171 (1995).
[16] R. Neutze, R. Wouts, D. van der Spoel, E. Weckert, and J. Hajdu, Nature (London) **406**, 752 (2000).
[17] K. Tamasaku, Y. Tanaka, M. Yabashi, H. Yamazaki, N. Kawamura, M. Suzuki, and T. Ishikawa, Nucl. Instrum. Methods Phys. Res. A **467-468**, 686 (2001).
[18] J. Miao, T. Ishikawa, E.H. Anderson, and K.O. Hodgson, Phys. Rev. B **67**, 174104 (2003).
[19] M. Yabashi, K. Tamasaku, and T. Ishikawa, Phys. Rev. Lett. **87**, 140801 (2001).